

Classification of tumor area using combined DCE and DSC MRI in patients with glioblastoma

Moran Artzi · Deborah T. Blumenthal ·
Felix Bokstein · Guy Nadav · Gilad Liberman ·
Orna Aizenstein · Dafna Ben Bashat

Received: 19 June 2014/Accepted: 18 October 2014/Published online: 5 November 2014
© Springer Science+Business Media New York 2014

Abstract This study proposes an automatic method for identification and quantification of different tissue components: the non-enhanced infiltrative tumor, vasogenic edema and enhanced tumor areas, at the subject level, in patients with glioblastoma (GB) based on dynamic contrast enhancement (DCE) and dynamic susceptibility contrast (DSC) MRI. Nineteen MR data sets, obtained from 12 patients with GB, were included. Seven patients were scanned before and 8 weeks following bevacizumab initiation. Segmentation of the tumor area was performed based on the temporal data of DCE and DSC at the group-level using *k*-means algorithm, and further at the subject-level using support vector machines algorithm. The obtained components were associated to different tissues types based on their temporal characteristics, calculated perfusion and permeability values and MR-spectroscopy. The method

enabled the segmentation of the tumor area into the enhancing permeable component; the non-enhancing hypoperfused component, associated with vasogenic edema; and the non-enhancing hyperperfused component, associated with infiltrative tumor. Good agreement was obtained between the group-level, unsupervised and subject-level, supervised classification results, with significant correlation ($r = 0.93$, $p < 0.001$) and average symmetric root-mean-square surface distance of 2.5 ± 5.1 mm. Longitudinal changes in the volumes of the three components were assessed alongside therapy. Tumor area segmentation using DCE and DSC can be used to differentiate between vasogenic edema and infiltrative tumors in patients with GB, which is of major clinical importance in therapy response assessment.

Keywords DCE · DSC · Tumor segmentation · Infiltrative tumor · Vasogenic edema

M. Artzi · G. Nadav · G. Liberman · O. Aizenstein ·
D. Ben Bashat (✉)
Functional Brain Center, The Wohl Institute for Advanced Imaging, Tel Aviv Sourasky Medical Center, 6 Weizman St, 64239 Tel Aviv, Israel
e-mail: dafnab@telmc.gov.il

M. Artzi · D. Ben Bashat
Sackler Faculty of Medicine, Tel Aviv University, Tel Aviv, Israel

D. T. Blumenthal · F. Bokstein
Neuro-Oncology Service, Tel Aviv Sourasky Medical Center, Tel Aviv, Israel

G. Nadav
Faculty of Engineering, Tel Aviv University, Tel Aviv, Israel

D. Ben Bashat
Sagol School of Neuroscience, Tel Aviv University, Tel Aviv, Israel

Introduction

Volumetric measurement of the enhancing tumor area in magnetic resonance imaging (MRI) is clinically important for diagnosis and therapy response assessment in patients with glioblastoma (GB). Due to the increased use of anti-angiogenic drugs, such as bevacizumab, for salvage therapies in these patients, recognition of changes in the hyperintense fluid attenuated inversion recovery (FLAIR) areas has been recommended in addition to quantification of the enhancing tumor area, as guidelines for therapy response assessment [1]. GB is the most common and most aggressive malignant primary brain tumor in humans, typically appears as a heterogeneous tumor on MRI, with tissue components including vasogenic edema, permeable

and non permeable (infiltrative) tumor areas [2]. Segmentation of tumor area and identification of changes not only in the overall tumor volume, but also in its different components, is of major clinical importance in therapy response assessment of these patients.

While the enhancing tumor area can relatively simply be identified based on conventional post contrast T₁ weighted images (T₁WI), differentiation between the infiltrative tumor area and vasogenic edema is more challenging. Both appear as non-enhancing areas with hyperintense signal in T₂WI/FLAIR. Due to the highly vascular profile of GB, vascular imaging methods seem to be suited to identify areas with infiltrative tumor.

Advanced vascular MRI methods provide information about tissue perfusion and permeability. Dynamic susceptibility contrast (DSC) is the most commonly used MR perfusion imaging and is considered the method of choice in clinical settings for the measurement of cerebral blood flow (CBF) and cerebral blood volume (CBV) [3–5]. CBV serves as an important imaging marker for brain tumor diagnosis, grading, and therapy response monitoring [6–8]. Dynamic contrast enhancement (DCE), also referred to as MR permeability imaging, provides several parameters regarding the tissue's vascular interstitial exchange, including the volume transfer constant (k^{trans}) [9]. This method has been previously used for tumor evaluation and therapy response assessment [10, 11].

Multi parametric imaging, provides comprehensive characterization of the tissue which can facilitate classification of the tumor into its different components. However, having multiple parameters complicates the extraction of diagnostic information across the images on a voxel basis, and necessitates the use of automatic or semi-automatic segmentation methods [12–16]. Automatic segmentation can be performed based on various imaging parameters extracted from the raw data or in the temporal domain; they can be categorized into supervised or unsupervised algorithms, and can either be performed at the group- or at the subject- level. Several studies have used the calculated DSC or DCE parameters for brain tumor segmentation [17–19]. However the extraction of the vascular parameters from the DSC and DCE data depends on several factors such as the choice of the tracer-kinetic modeling and arterial input function (AIF) [9, 20–23], and thus affects segmentation results. Analysis in the temporal domain, although depends on acquisition parameters, may overcome some of the issues relating to the analysis process. In addition, most studies which aimed to classify the tumor area in patients with GB performed group-level analysis, which is less suitable for clinical setup, where classification of the individual patient's data set is required.

In this study we segmented the tumor area in patients with GB into components with clinical importance, based

on combined DCE and DSC MR data. We aimed to quantify the enhancing tumor area and differentiate between tumor-infiltrative area and vasogenic edema, providing a tool for subject-level segmentation. The applicability of the method is shown in patients with GB with the ability to monitor changes in tumor components during bevacizumab therapy.

Materials and methods

Patients

A total of 19 MR data sets, obtained from twelve patients with recurrent GB (7 men, mean age 53 ± 14 years), who were candidates to receive bevacizumab therapy were included. All patients had been treated with standard therapies of surgery, radiation and chemotherapy prior to bevacizumab therapy. Only patients who had both DCE and DSC data with sufficient overlap of brain coverage between methods were included. Data of patients with severe motion artifacts or significantly different imaging parameters (such as the acquired temporal resolution of DCE/DSC, injection rate, and others) were not included in this study. Seven patients, receiving bevacizumab as a second-line therapy, were scanned before (baseline) and 8 weeks following therapy initiation. Other inclusion criteria were normal glomerular filtration rate and no contraindication to MRI. All patients were previously treated with standard first-line therapies of surgery, radiation and chemotherapy. The study was approved by the hospital review board, and written informed consent was obtained from all patients.

Imaging protocol

MRI scans were performed on a 3.0 Tesla MRI scanner (GE Signa EXCITE, Milwaukee, WI, USA) using an eight channel head coil. The protocol included: high-resolution T₁WI fast spoiled gradient echo (SPGR) performed before and after contrast agent injection (field of view (FOV/matrix) = 256 mm/256 × 256, repetition time (TR)/echo time (TE) = 9.0–5.3/3.5–1.3 ms); FLAIR (FOV/matrix = 240 mm/256 × 256, TR/TE/inversion time = 10,000–9,000/146–117/2,500–2,100 ms); diffusion tensor imaging (DTI) (FOV/matrix = 250–240 mm/96 × 96; TR/TE = 12,000–8,000/98–87 ms, 19 gradient directions, b-value = 0 and 1,000 s/mm²); DCE data, acquired using multi phase 3D T₁WI SPGR imaging during the injection of 0.2 cc/kg contrast agent, using a power injector, followed by a flush of 20 cc saline, both at a constant rate of 5 cc/sec (FOV/matrix = 250 mm/256 × 256, TR/TE = 5.68/1.24 ms, flip angles (FA) = 30°). For the T₁ maps, variable flip angle SPGR

(VFA-SPGR) data was acquired with FAs = 5°/10°/15°/25°. Slices were located at the center of the tumor area (as defined based on the anatomical images), and DSC (FOV/matrix = 220–240 mm/128 × 128, TR/TE = 1,300/30 ms and 78–92 repetitions), acquired using a 2D gradient echo, echo planar imaging (GRE-EPI) sequence during the injection of Gadolinium-Dotarem. A power injector (MEDRAD, Spectris Solaris EP) was used to infuse 0.4 cc/kg (a double dose) of contrast agent with a delay of 15 s, followed by a flush of 20 cc saline, both at a constant rate of 5 cc/sec. MR spectroscopy (MRS) was acquired using 2D multi voxel point resolved spectroscopy chemical shift imaging (PRESS CSI) sequence, with 16 × 16 transverse phase encoding matrix, TR/TE = 1,500/144 ms, placed at the center of the tumor area.

Data analysis

Data preprocessing

Included coregistration, skull stripping and bias field correction. *Coregistration* in each patient all images, FLAIR, post contrast T₁WI, DSC raw data and calculated maps (at both time points when available), were realigned to the DCE data using FSL affine registration tool [24]. *Skull stripping* was performed using FSL brain extraction tool. *Bias field correction* was applied to the T₁WI and FLAIR images, using Freesurfer N3 MINC B₀ non uniformity correction tool.

Volumes of interest (VOIs) identification

Two VOIs were defined: (a) The target tumor area for segmentation (VOI1), defined as the union of hyperintense FLAIR and the hyperintense post contrast T₁WI areas, identified using previously described methodology [25], and (b) The contra-lateral normal appearing white matter (NAWM, VOI2) to be served as a reference area. VOI2 was defined by flipping VOI1 to the contra-lateral hemisphere, and was masked by the NAWM area, defined by FLAIR, T₁WI and the DSC data based on [26]. In order to minimize partial volume effect and exclude voxels associated with tissue necrosis, voxels with mean diffusivity values within two standard deviations of that of the cerebral spinal fluid (CSF), were excluded in both VOI1 and VOI2.

Unsupervised group-level segmentation

Unsupervised segmentation of the target tumor area was performed with *k*-means algorithm, using Matlab. The input data was preprocessed concatenated DCE and DSC

raw data, obtained from all scans (n = 19). The algorithm was run with the number of clusters, *k* = 3–10, and the final *k* was set following analysis optimization, based on the elbow method. Preprocessing included removal of the first three time points in each data set and intensity normalization, performed separately for each data set relative to baseline. In order to reduce the number of points and use only those which contributed to the differences between components, only 15 data points were used in the DCE and 16 in the DSC, around the volume of maximum signal change (ΔS). The selected data points were concatenated, and used as input data for segmentation.

Map calculation

The volume transfer constant (k^{trans}) maps were calculated from the DCE data, using in-house code written in MATLAB based on extended Tofts model [27] using flip angle correction for the T₁ calculations [28]. The CBV and CBF maps were calculated from the DSC data, using the PEr-fusioN Graphical User INterface (Penguin, <http://cfin.au.dk/>) software, and normalized values (rCBV, rCBF) were calculated relative to the contra-lateral NAWM (VOI2). Mean diffusivity maps were calculated from the DTI data, using the FSL Diffusion Toolbox. The Choline to Cr (Cho/Cr) ratio values were calculated from the MRS data, by the standard GE Functool software.

Evaluation of the results

Mean k^{trans} , rCBV, rCBF, and Cho/Cr values were calculated in the different components. Differences in the permeability and perfusion values between components were assessed using one way ANOVA with correction for multiple comparisons. Cho/Cr values were used to evaluate the differences between components.

Supervised subject-level segmentation

We further evaluated the ability of the method to be used for classification of unseen single-subject data, using support vector machine (SVM) algorithm, using Matlab. A form of twofold cross validation was used. Initially the entire database was partitioned into two groups (n₁ = 9, n₂ = 10) based on even odd case selection. A *k*-means segmentation was applied separately on the even or odd data sets, with the optimized *k* number. The *k*-means segmentation results in one group were used as a training set for the SVM algorithm, applied separately to each MR data set (the preprocessed concatenated DCE and DSC data) from the other group.

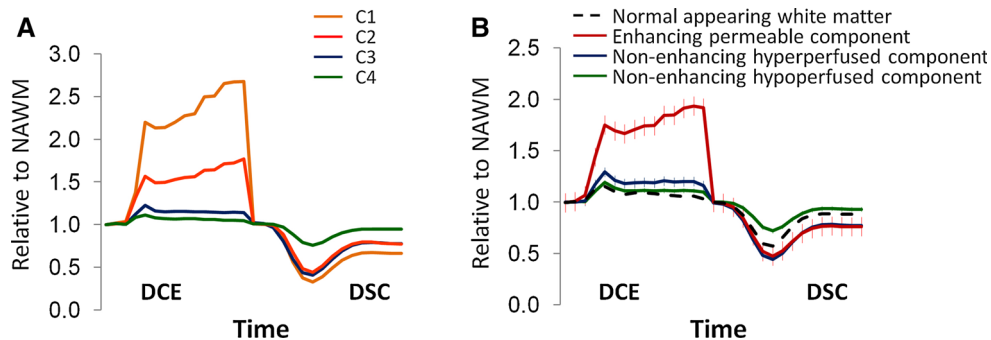


Fig. 1 Time curves of the DCE and DSC data obtained following k -means segmentation. **a** the obtained clusters centroids, **b** the mean and standard error of the signal time curves obtained from all scans for the

three tissue components and for the normal appearing white matter (NAWM). All signal time curves are given in percentages relative to the pre-contrast images

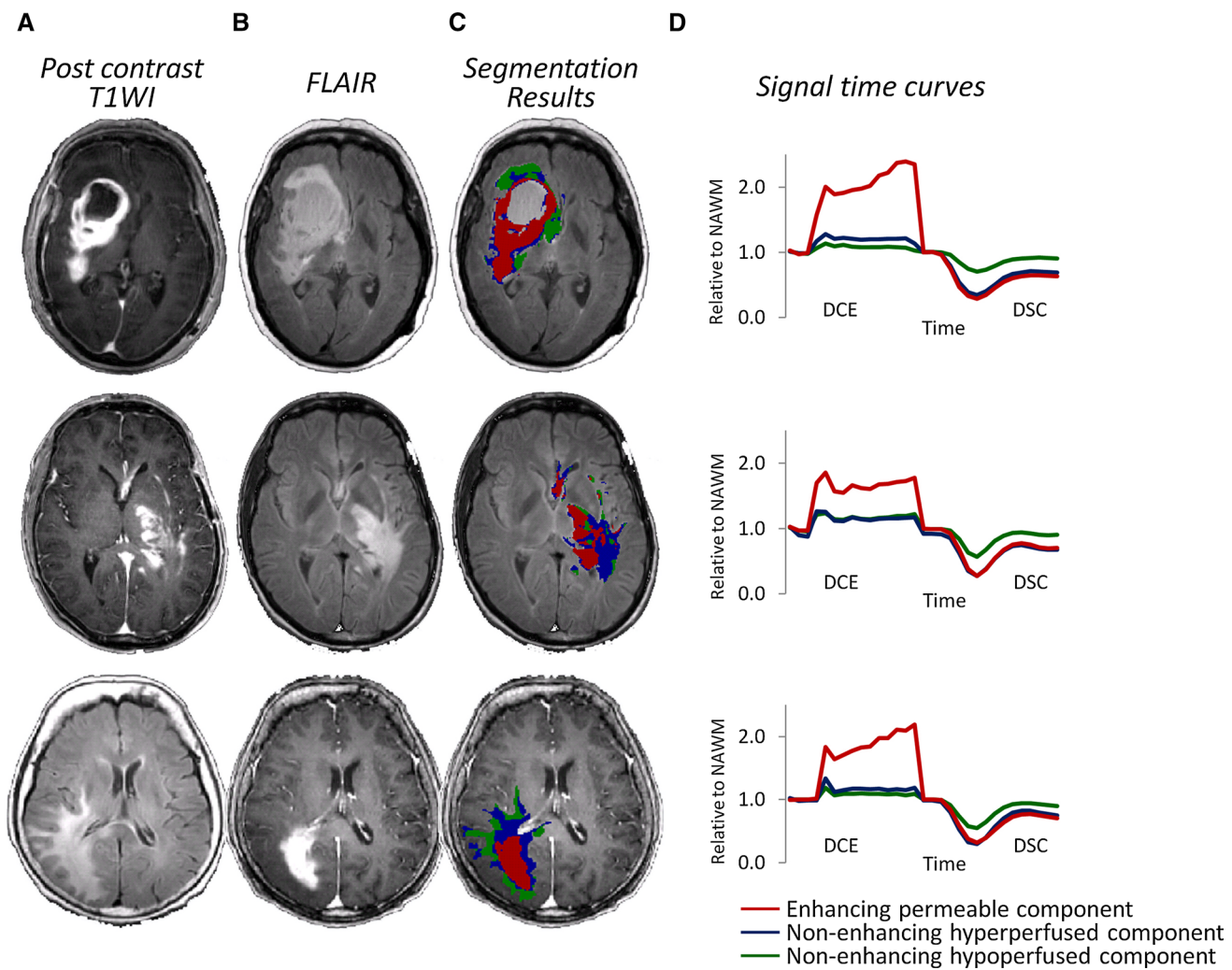


Fig. 2 Representative data obtained from three patients showing **a** post contrast T₁ weighted images (WI), **b** FLAIR images, **c** the obtained k -means tumor segmentation results, and **d** the time curves of the DCE and DSC data obtained for the three components in each patient

Comparisons between the volume and the spatial overlap of the components obtained using group- and subject-level segmentations were performed using Pearson correlation and based on [29].

Results

The target tumor area for segmentation (VOI1) was identified in all patients. The volume of the T₁ WI post contrast

area was: mean = $20.6 \pm 17.3 \text{ cc}^3$, range = 1.6–60.3 cc^3 ; and the hyperintense FLAIR lesion area was: mean = $35.6 \pm 19.9 \text{ cc}^3$, range: 9.1–75.7 cc^3 .

Unsupervised group-level segmentation results

Following optimization, the k number used for tumor segmentation was set to four. Figure 1a shows the mean concatenated data obtained from each cluster. The obtained clusters were labeled and grouped based on their temporal characteristics. As cluster number 1 (C1) and C2 both demonstrated progressive signal increment following the bolus passage on the DCE data, indicating high tissue permeability, and a larger signal drop on DSC, indicating high CBV values. Therefore, these two clusters were combined and referred to as the *enhancing permeable component*. C3 demonstrated no substantial increase in signal following the bolus passage on the DCE data, thus indicating no permeability, and a large DSC signal drop, similar to that observed for C1 and C2. This cluster was referred to as the *non-enhancing hyperperfused component*. C4 demonstrated no tissue permeability on the DCE data, and a lower DSC signal drop relative to the other components, and to the NAWM, and was thus referred to as a *non-enhancing hypoperfused component* (Fig. 1b). Segmentation results obtained in three patients are shown in Fig. 2.

Evaluation of the results

We further associated the different components into different tissue types based on their permeability (k^{trans}) and perfusion (rCBV, rCBF) values, MRS results, and previous studies [6, 30, 31]. The mean k^{trans} , rCBV and rCBF values detected in the contra-lateral NAWM and in the three obtained components are presented in Table 1. The *enhancing permeable* component had significantly higher permeability (k^{trans}) than the other two components and the NAWM, and a mean high rCBV (>1.75) and rCBF, compared to the NAWM and to the *non-enhancing hyperperfused* component. Therefore this component was associated with active tumor. The *non-enhancing hyperperfused* component was significantly different from the *non-enhancing hypoperfused*, and was characterized by rCBV values >1.75 relative to NAWM. This value was suggested previously as a threshold indicating high grade tumors [6, 32], and thus, this component was associated with infiltrative tumor. The *non-enhancing hypoperfused* component was characterized by no increased permeability compared to the NAWM, and with the lowest rCBV and rCBF values, significantly differing from the other two components and from the NAWM. This perfusion pattern was associated with vasogenic edema in previous studies [30, 31], and thus

referred in this study as vasogenic edema. A scatter plot of k^{trans} , rCBV and rCBF values, obtained for the NAWM, and the three components is presented in Fig. 3, demonstrating a clear separation between components.

Twenty MR spectra were obtained in seven scans, supported the association between the obtained components and the associated tissue state. The *non-enhancing hypoperfused* component, associated with vasogenic edema, had Cho/Cr values of 1.19 ± 0.09 similar to that of the NAWM (1.13 ± 0.10), while the *enhancing permeable* and the *non-enhancing hyperperfused* components, associated with the active and infiltrative tumor areas, had high Cho/Cr values (2.18 ± 0.68 , and 1.51 ± 0.13 , respectively). Such high values have been associated with areas of infiltrative tumor cells [33].

Subject-level segmentation results

The ability to segment the tumor area of unseen data at the subject level was assessed using SVM algorithm, with the k -means segmentation results used as a training set for the classification process. A good agreement was detected between methods, with average symmetric root mean square surface distance of $2.5 \pm 5.7 \text{ mm}$ and Pearson correlation of $r = 0.93$, $p < 0.001$. Figure 4 shows results obtained in two patients with GB using group-level k -mean and subject-level SVM segmentations, demonstrating.

Longitudinal assessment

Eight weeks following therapy initiation, the total tumor volume (hyperintense FLAIR and the enhanced T₁WI areas) showed a decrease in 4/7 patients, (range of 40–79 %), no substantial change (<10 %) in two patients and an increase (29 %) only in one patient. However, this pattern of reduction/stability (no change) in the total tumor volume was contributed mainly by a reduction in the volume of the *vasogenic edema* detected in 6/7 patients, (range of 33–82 %), with one patient showing no change (2 %), along with an increase in the volume of one or both of the other tumor components: the *enhancing permeable* and *non-enhancing hyperperfused* components. For example, in two cases no substantial change in the volume of the hyperintense FLAIR lesion area was detected indicating stable disease, yet a significant increase in the infiltrative tumor area was detected supporting progressive disease.

Discussion

Tumor area segmentation was performed in patients with GB based on temporal analysis of DCE and DSC data. The obtained components were labeled and associated with

Table 1 MRI parameters obtained for the different components

	rCBV (a.u.)	rCBF (a.u.)	k^{trans} (1/min)
Contra-lateral normal appearing white matter	1.00 ± 0.00 ^{b,c,d}	1.00 ± 0.00 ^{b,c,d}	0.0034 ± 0.0047 ^{c,d}
Enhancing permeable component	2.46 ± 1.00 ^{a,b}	1.46 ± 0.53 ^{a,b}	0.0749 ± 0.0443 ^{a,b,c}
Non-enhancing hyperperfused component	1.80 ± 0.43 ^{a,b}	1.34 ± 0.32 ^{a,b}	0.0144 ± 0.0093 ^{a,d}
Non-enhancing hypoperfused component	0.68 ± 0.16 ^{a,c,d}	0.62 ± 0.18 ^{b,c,d}	0.0090 ± 0.0061 ^d

Means and standard deviations of perfusion and permeability values obtained in the three components compared to the normal appearing white matter (NAWM); rCBV, rCBF = cerebral blood volume, flow, relative to the contra-lateral NAWM (in arbitrary units (a.u.)). k^{trans} = permeability index (1/min)

Significant ($p < 0.05$) differences were obtained from

^a NAWM

^b Non-enhancing hypoperfused component

^c Non-enhancing hyperperfused component

^d Enhanced permeable component

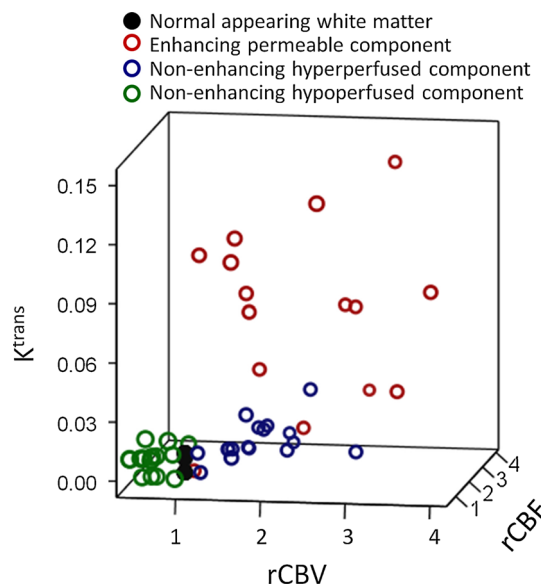


Fig. 3 Three dimensional scatter plot of the k^{trans} , relative CBV (rCBV), and relative CBF (rCBF) values, obtained from the normal appearing white matter, and from the three components from all data sets ($n = 19$)

tissues of clinical importance: the *enhancing permeable component*; the *non-enhancing hyperperfused component*, associated with infiltrative tumor area; and the *non-enhancing hypoperfused component*, associated with vasogenic edema. These components were significantly different from each other in their temporal patterns and perfusion/permeability values. The associations between the obtained components and tissue state were based on their perfusion and permeability patterns and based on previously reported studies [6, 30, 31, 33, 34], supported by MRS. The applicability of the proposed method for the classification of unseen single-subject data was demonstrated using SVM algorithm.

Previously, therapy response assessment in patients with GB was based on 2-dimensional measurement of the contrast enhancing tumor area alone. Accumulated evidence in recent years demonstrates the limitations of these criteria, especially for the assessment of anti-angiogenic therapy response. In 2010, the revised assessment in neuro-oncology (RANO) criteria was proposed [1], addressing the importance of qualitative assessment of the non enhancing tumor area as seen on FLAIR/T₂WI, in addition to quantitative assessment of the enhanced tumor volume. However, it is not clear whether a hyperintense FLAIR lesion area represents vasogenic edema or infiltrative tumor area, or a combination of the two. While the identification of the enhancing tumor area is relatively simple, the differentiation between the vasogenic edema and the non-enhancing infiltrative tumor area, is more challenging, yet highly important for the assessment of patients with GB, in particular for therapy response monitoring of anti-angiogenic treatments [1]. Only a few studies have attempted to classify the non-enhancing lesion area into infiltrative tumor versus vasogenic edema [13, 35, 36], and only a limited use was previously made of advanced imaging, especially vascular methods.

Due to the highly vascular nature of GB tumors, perfusion and permeability imaging have been shown to provide important information for tumor classification and therapy response assessment [37]. Although DCE and DSC have been extensively used in research and clinical settings, there are several difficulties regarding extracting the perfusion and permeability parameters from these methods [9, 21, 23]. Quantification of cerebral permeability from DCE data relays on tracer-kinetic modeling, which necessitates assumptions about the model [9], requires accurate T₁ measurements and does not take into account differences in blood flow and bolus arrival time [21]. High CBF is often misinterpreted as high permeability [22]. For the

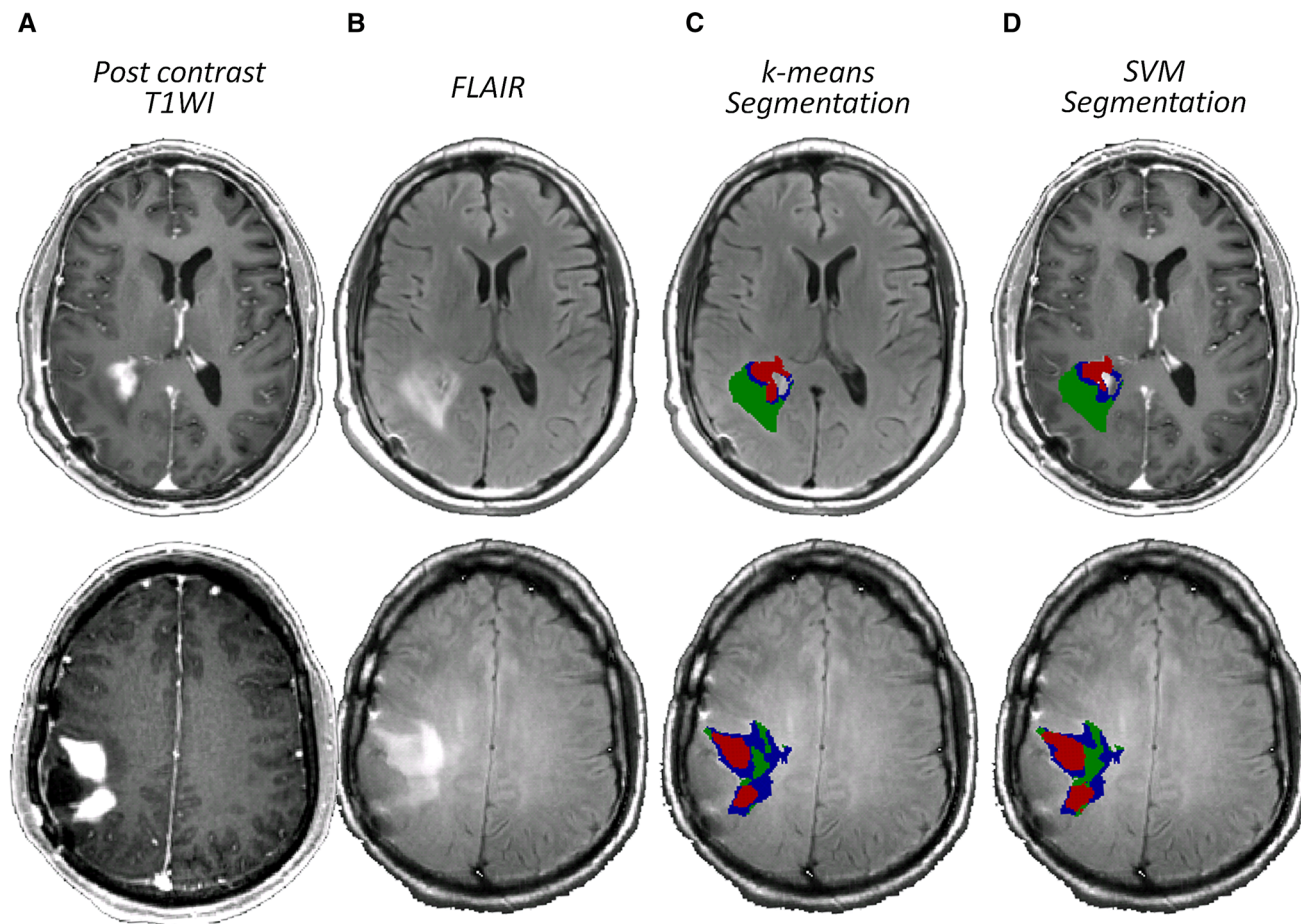


Fig. 4 Comparison of segmentation methods. **a** post contrast T1 weighted images (WI), **b** FLAIR **c** group-level *k*-means, and **d** subject-level SVM segmentation results obtained from two patients

with GB. *Green* the non-enhancing hypoperfused component, *blue* the non-enhancing hyperperfused component *red* the enhancing permeable component

DSC data, quantification of cerebral perfusion usually relies on the assumption of an intact blood brain barrier (BBB) which is not the case in GB. This is known to be a major source of error, leading to inaccurate estimation of CBV and CBF [20]. In addition, in both methods, the calculated parameters depend on the chosen AIF [9, 23]. Analysis in the temporal domain may overcome some of the dependency on the analysis process, although it may be more sensitive to scanning parameters. A few studies have performed tumor segmentation in the temporal domain using independent component analysis of DSC MRI to measure perfusion patterns [38], and to predict anti-angiogenic therapy response [39] in patients with brain tumors. However, to the best of our knowledge, no previous study has performed tumor segmentation in the temporal domain based on combined vascular imaging methods.

Segmentation results were characterized by the DCE and DSC temporal characteristics relative to the NAWM, and further associated to clinically important tissue types based on their perfusion, permeability values, MRS, and

previous studies [6, 30, 31]. The segmentation process was initially performed at the group-level ($n = 19$), using unsupervised *k*-means algorithm. The major advantages of this algorithm are its simplicity and speed, which allow its use on a large data set. However, while reinforcing the statistical power of the data analysis, the group-level segmentation is unsuitable for clinical needs. Therefore, a subject-level analysis was further performed based on SVM algorithm, trained based on the group-level *k*-means segmentation results. The good agreement between the two methods demonstrated the potential of the proposed methodology to be used in clinical settings for tumor segmentation, once a training data set is acquired.

A longitudinal study was performed in a sub-group of patients with GB receiving bevacizumab therapy. Our results are in line with previous reports, showing that bevacizumab can produce a marked radiologic response with reduction of total tumor volume, however this response is largely a result of reduced vascular permeability and vasogenic edema rather than a true anti-tumor effect [1]. In several patients with stable volume of FLAIR

hyperintense area over time, increased volume of infiltrative tumor component accompanied reduction in the total non-enhancing tumor area and/or vasogenic edema (sumstable hyperintensity), indicating disease progression rather than stable disease as would have been diagnosed based on RANO criteria alone. This finding highlights the importance of distinguishing between the different elements of the hyperintense FLAIR lesion: vasogenic edema versus infiltrative tumor area, to improve therapy response assessment.

In this study the enhancing tumor area was viewed as one component associated with active tumor, based on its mean high rCBV and rCBF values. However, this component may be composed of two distinct tissue types; active tumor and area of tissue necrosis (radiation–necrosis). Differentiation between recurrent tumor versus pseudo-progression is important in therapy response assessment. Future studies should attempt to differentiate between these components. In addition, the non-enhancing tumor area (the hyperintense FLAIR lesion area) was segmented into two entities: a non-enhancing hypoperfused component associated with vasogenic edema, and non-enhancing hyperperfused component associated with infiltrative tumor. It is important to note that due to the highly infiltrative nature of GB tumors, GB cells may also spread to areas not defined as hyperintense in FLAIR images. In addition, within the hyperintense FLAIR area, a graded pattern of infiltration is expected rather than a clearly defined border between the two components. However for simplicity, and to facilitate clinical assessment of disease progression/therapy response, segmentation into two components was performed.

Several limitations to this study should be considered. The association between the obtained segmentation results and the tissue type was based on their MRI characteristics, supported by MRS findings and literature. In the absence of histological evidence these results lack gold-standard for validation, yet it is important to note that histology is generally unavailable in patients with progressive disease. In addition, a correction for leakage was not performed in the DSC analysis. This may result in underestimation of CBV values in areas with impaired BBB. This may affect our results within the enhancing tumor, leading to lower estimation of CBV values, yet strengthens our results and confirms the malignant pattern of this component. However, not correcting for leakage is not expected to effect the segmentation between the vasogenic edema and infiltrative tumor and their perfusion values, as these components are non-enhancing.

In conclusion, this study shows the feasibility of segmentation of the tumor area in patients with GB receiving anti-angiogenic therapy. Segmentation was performed in the temporal domain based on combined DCE and DSC

data, both at the group-level using an unsupervised algorithm and further applied at the subject-level using a supervised algorithm. The proposed methodology enables differentiation between vasogenic edema and infiltrative tumor, which is important in the diagnosis and therapy response assessment of patients with high grade brain tumors.

Acknowledgments To Guy Nadav for technical support and to Vicki Myers for editorial assistance. This work was performed in partial fulfillment of the requirements for a Ph.D. degree of Artzi Moran, Sackler Faculty of Medicine, Tel Aviv University, Israel.

Conflict of interest We declare that there is no conflict of interest for any of the authors.

Funding This work was supported by the James S. McDonnell Foundation number 220020176.

References

- Wen PY, Macdonald DR, Reardon DA, Cloughesy TF, Sorensen AG, Galanis E, Degroot J, Wick W, Gilbert MR, Lassman AB, Tsien C, Mikkelsen T, Wong ET, Chamberlain MC, Stupp R, Lamborn KR, Vogelbaum MA, van den Bent MJ, Chang SM (2010) Updated response assessment criteria for high-grade gliomas: response assessment in neuro-oncology working group. *J Clin Oncol* 28:1963–1972. doi:[10.1200/JCO.2009.26.3541](https://doi.org/10.1200/JCO.2009.26.3541)
- Demir MK, Hakan T, Akinci O, Berkman Z (2005) Primary cerebellar glioblastoma multiforme. *Diagn Interv Radiol* 11:83–86
- Ostergaard L, Sorensen AG, Kwong KK, Weisskoff RM, Gyldenstedt C, Rosen BR (1996) High resolution measurement of cerebral blood flow using intravascular tracer bolus passages. Part II: experimental comparison and preliminary results. *Magn Reson Med* 36:726–736
- Ostergaard L, Weisskoff RM, Chesler DA, Gyldenstedt C, Rosen BR (1996) High resolution measurement of cerebral blood flow using intravascular tracer bolus passages. Part I: mathematical approach and statistical analysis. *Magn Reson Med* 36:715–725
- Sourbron S, Ingrisch M, Sievert A, Reiser M, Herrmann K (2009) Quantification of cerebral blood flow, cerebral blood volume, and blood-brain-barrier leakage with DCE-MRI. *Magn Reson Med* 62:205–217. doi:[10.1002/mrm.22005](https://doi.org/10.1002/mrm.22005)
- Al-Okaili RN, Krejza J, Wang S, Woo JH, Melhem ER (2006) Advanced MR imaging techniques in the diagnosis of intraaxial brain tumors in adults. *Radiographics* 26(Suppl 1):S173–S189. doi:[10.1148/radio.26si065513](https://doi.org/10.1148/radio.26si065513)
- Cha S (2006) Update on brain tumor imaging: from anatomy to physiology. *AJNR Am J Neuroradiol* 27:475–487
- Fatterpekar GM, Galheigo D, Narayana A, Johnson G, Knopp E (2012) Treatment-related change versus tumor recurrence in high-grade gliomas: a diagnostic conundrum—use of dynamic susceptibility contrast-enhanced (DSC) perfusion MRI. *AJR Am J Roentgenol* 198:19–26. doi:[10.2214/AJR.11.7417](https://doi.org/10.2214/AJR.11.7417)
- Sourbron SP, Buckley DL (2013) Classic models for dynamic contrast-enhanced MRI. *NMR Biomed* 26:1004–1027. doi:[10.1002/nbm.2940](https://doi.org/10.1002/nbm.2940)
- Zhang W, Kreisl TN, Solomon J, Reynolds RC, Glen DR, Cox RW, Fine HA, Butman JA (2009) Acute Effects of Bevacizumab on Glioblastoma Vascularity Assessed with DCE-MRI and Relation to Patient Survival. The International Society for Magnetic Resonance in Medicine, Honolulu

11. Sorensen AG, Batchelor TT, Zhang WT, Chen PJ, Yeo P, Wang M, Jennings D, Wen PY, Lahdenranta J, Ancukiewicz M, di Tomaso E, Duda DG, Jain RK (2009) A “vascular normalization index” as potential mechanistic biomarker to predict survival after a single dose of cediranib in recurrent glioblastoma patients. *Cancer Res* 69:5296–5300. doi:[10.1158/0008-5472.CAN-09-0814](https://doi.org/10.1158/0008-5472.CAN-09-0814)
12. Huo J, Okada K, van Rikxoort EM, Kim HJ, Alger JR, Pope WB, Goldin JG, Brown MS (2013) Ensemble segmentation for GBM brain tumors on MR images using confidence-based averaging. *Med Phys* 40:093502. doi:[10.1111/1.4817475](https://doi.org/10.1111/1.4817475)
13. Liberman G, Louzoun Y, Aizenstein O, Blumenthal DT, Bokstein F, Palmon M, Corn BW, Ben Bashat D (2013) Automatic multimodal MR tissue classification for the assessment of response to bevacizumab in patients with glioblastoma. *Eur J Radiol* 82:e87–e94. doi:[10.1016/j.ejrad.2012.09.001](https://doi.org/10.1016/j.ejrad.2012.09.001)
14. Wu W, Chen AY, Zhao L, Corso JJ (2013) Brain tumor detection and segmentation in a CRF (conditional random fields) framework with pixel-pairwise affinity and superpixel-level features. *Int J Comput Assist Radiol Surg*. doi:[10.1007/s11548-013-0922-7](https://doi.org/10.1007/s11548-013-0922-7)
15. Zhu Y, Young GS, Xue Z, Huang RY, You H, Setayesh K, Hatabu H, Cao F, Wong ST (2012) Semi-automatic segmentation software for quantitative clinical brain glioblastoma evaluation. *Acad Radiol* 19:977–985. doi:[10.1016/j.acra.2012.03.026](https://doi.org/10.1016/j.acra.2012.03.026)
16. Assefa D, Keller H, Menard C, Laperriere N, Ferrari RJ, Yeung I (2010) Robust texture features for response monitoring of glioblastoma multiforme on T1-weighted and T2-FLAIR MR images: a preliminary investigation in terms of identification and segmentation. *Med Phys* 37:1722–1736
17. Zollner FG, Emblem KE, Schad LR (2010) Support vector machines in DSC-based glioma imaging: suggestions for optimal characterization. *Magn Reson Med* 64:1230–1236. doi:[10.1002/mrm.22495](https://doi.org/10.1002/mrm.22495)
18. Emblem KE, Nedregård B, Hald JK, Nome T, Due-Tonnessen P, Bjørnerud A (2009) Automatic glioma characterization from dynamic susceptibility contrast imaging: brain tumor segmentation using knowledge-based fuzzy clustering. *J Magn Reson Imaging* 30:1–10. doi:[10.1002/jmri.21815](https://doi.org/10.1002/jmri.21815)
19. Singh A, Rathore R, Gupta R, Haris M, Rathore DK, Verma SK, Purwar A, Bayu G, Sarma MK, Singh JK (2007) Segmentation of Gd-DTPA Enhancing Lesion of Brain using Time to Peak of Concentration Time Curve and its Pharmacokinetic Analysis in Dynamic Contrast Enhanced (DCE) MRI. The International Society for Magnetic Resonance in Medicine, Berlin
20. Vonken EP, van Osch MJ, Bakker CJ, Viergever MA (2000) Simultaneous quantitative cerebral perfusion and Gd-DTPA extravasation measurement with dual-echo dynamic susceptibility contrast MRI. *Magn Reson Med* 43:820–827. doi:[10.1002/1522-2594\(200006\)43:6<820::AID-MRM7>3.0.CO;2-F](https://doi.org/10.1002/1522-2594(200006)43:6<820::AID-MRM7>3.0.CO;2-F)
21. Bagher-Ebadian H, Jain R, Nejad-Davarani SP, Mikkelsen T, Lu M, Jiang Q, Scarpace L, Arbab AS, Narang J, Soltanian-Zadeh H, Paudyal R, Ewing JR (2012) Model selection for DCE-T1 studies in glioblastoma. *Magn Reson Med* 68:241–251. doi:[10.1002/mrm.23211](https://doi.org/10.1002/mrm.23211)
22. Nadav G, Liberman G, Artzi M, Kiryati N, Ben Bashat D (2014) Flow and permeability estimation from DCE data: 2-compartment exchange and Tofts models comparison. The International Society for Magnetic Resonance in Medicine, Milan
23. Calamante F (2013) Arterial input function in perfusion MRI: a comprehensive review. *Prog Nucl Magn Reson Spectrosc* 74:1–32. doi:[10.1016/j.pnmrs.2013.04.002](https://doi.org/10.1016/j.pnmrs.2013.04.002)
24. Smith SM, Jenkinson M, Woolrich MW, Beckmann CF, Behrens TE, Johansen-Berg H, Bannister PR, De Luca M, Drobniak I, Flitney DE, Niazy RK, Saunders J, Vickers J, Zhang Y, De Stefano N, Brady JM, Matthews PM (2004) Advances in functional and structural MR image analysis and implementation as FSL. *Neuroimage* 23(Suppl 1):S208–S219. doi:[10.1016/j.neuroimage.2004.07.051](https://doi.org/10.1016/j.neuroimage.2004.07.051)
25. Artzi M, Aizenstein O, Jonas-Kimchi T, Myers V, Hallevi H, Ben Bashat D (2013) FLAIR lesion segmentation: application in patients with brain tumors and acute ischemic stroke. *Eur J Radiol* 82:1512–1518. doi:[10.1016/j.ejrad.2013.05.029](https://doi.org/10.1016/j.ejrad.2013.05.029)
26. Artzi M, Aizenstein O, Hendlir T, Ben Bashat D (2011) Unsupervised multiparametric classification of dynamic susceptibility contrast imaging: study of the healthy brain. *Neuroimage* 56:858–864. doi:[10.1016/j.neuroimage.2011.03.027](https://doi.org/10.1016/j.neuroimage.2011.03.027)
27. Tofts PS, Kermode AG (1991) Measurement of the blood-brain barrier permeability and leakage space using dynamic MR imaging. 1. Fundamental concepts. *Magn Reson Med* 17:357–367
28. Liberman G, Louzoun Y, Colliot O, BB D (2011) T1 mapping, AIF and pharmacokinetic parameter extraction from dynamic contrast enhancement MRI data. *Multimodal Brain Image Anal* 7012:76–83
29. Gerig G, Jomier M, Chakos M (2001) Valmet: a new validation tool for assessing and improving 3D object segmentation. MICCAI, Beijing
30. Hossman KA, Bloink M (1981) Blood flow and regulation of blood flow in experimental peritumoral edema. *Stroke* 12:211–217
31. Law M, Cha S, Knopp EA, Johnson G, Arnett J, Litt AW (2002) High-grade gliomas and solitary metastases: differentiation by using perfusion and proton spectroscopic MR imaging. *Radiology* 222:715–721. doi:[10.1148/radiol.2223010558](https://doi.org/10.1148/radiol.2223010558)
32. Law M, Yang S, Wang H, Babb JS, Johnson G, Cha S, Knopp EA, Zagzag D (2003) Glioma grading: sensitivity, specificity, and predictive values of perfusion MR imaging and proton MR spectroscopic imaging compared with conventional MR imaging. *AJR Am J Neuroradiol* 24:1989–1998
33. Croteau D, Scarpace L, Hearshen D, Gutierrez J, Fisher JL, Rock JP, Mikkelsen T (2001) Correlation between magnetic resonance spectroscopy imaging and image-guided biopsies: semiquantitative and qualitative histopathological analyses of patients with untreated glioma. *Neurosurgery* 49:823–829
34. Law M, Yang S, Babb JS, Knopp EA, Golfinos JG, Zagzag D, Johnson G (2004) Comparison of cerebral blood volume and vascular permeability from dynamic susceptibility contrast-enhanced perfusion MR imaging with glioma grade. *AJR Am J Neuroradiol* 25:746–755
35. Lu S, Ahn D, Johnson G, Law M, Zagzag D, Grossman RI (2004) Diffusion-tensor MR imaging of intracranial neoplasia and associated peritumoral edema: introduction of the tumor infiltration index. *Radiology* 232:221–228. doi:[10.1148/radiol.2321030653](https://doi.org/10.1148/radiol.2321030653)
36. Kinoshita M, Goto T, Okita Y, Kagawa N, Kishima H, Hashimoto N, Yoshimine T (2010) Diffusion tensor-based tumor infiltration index cannot discriminate vasogenic edema from tumor-infiltrated edema. *J Neurooncol* 96:409–415. doi:[10.1007/s11060-009-9979-0](https://doi.org/10.1007/s11060-009-9979-0)
37. Pope WB, Young JR, Ellingson BM (2011) Advances in MRI assessment of gliomas and response to anti-VEGF therapy. *Curr Neurol Neurosci Rep* 11:336–344. doi:[10.1007/s11910-011-0179-x](https://doi.org/10.1007/s11910-011-0179-x)
38. LaViolette PS, Cohen AD, Rand SD, Mueller W, Schmainda KM (2011) Independent component analysis of dynamic susceptibility contrast MRI in brain tumor: a new biomarker for measuring tumor perfusion patterns. The International Society for Magnetic Resonance in Medicine, Montreal
39. LaViolette PS, Cohen AD, Prah MA, Rand SD, Connelly J, Malkin MG, Mueller WM, Schmainda KM (2013) Vascular change measured with independent component analysis of dynamic susceptibility contrast MRI predicts bevacizumab response in high-grade glioma. *Neuro Oncol* 15:442–450. doi:[10.1093/neuonc/nos323](https://doi.org/10.1093/neuonc/nos323)